Surface Functionalized Vapor Grown Carbon Fiber Supported Dysprosium Stannate Composites for the Enhanced Detection of Furaltadone: A Synergy of DFT Modeling and Experiment

Farhana Yasmin Rahman[a,b,c], Rajendran Surya[b,c], Konstantin Katin[d], Shu Yin[e,f], Syed Arshad Hussain[a], Subramanian Sakthinathan[b,c]*, Te-Wei Chiu[b,c]*

[a]Thin Film and Nanoscience Laboratory, Department of Physics, Tripura University (Suryamaninagar-799022), Tripura, India.

[b]Department of Materials and Mineral Resources Engineering, National Taipei University of Technology, No. 1, Sec. 3, Zhongxiao E. Rd., Taipei 10608 Taiwan.

[c]Institute of Materials Science and Engineering, National Taipei University of Technology, No. 1, Sec. 3, Zhongxiao E. Rd., Taipei 10608 Taiwan.

[d]Laboratory of 2D Nanomaterials in Electronics, Photonics and Spintronics, National Research Nuclear University "MEPhI", 31 Kashirskoe sh., Moscow, 115409, Russian Federation.

[e] Institute for Multidisciplinary Research for Advanced Materials, Tohoku University, 2-1-1 Katahira, Aoba-ku, Sendai 980-8577, Japan.

[f]Advanced Institute for Materials Research (WPI-AIMR), Tohoku University, 2-1-1 Katahira, Aoba-ku, Sendai, Miyagi 980-8577, Japan.

Corresponding author: Te-wei Chiu; tewei@ntut.edu.tw. Sakthinathan Subramanian; sakthinathan1988@gmail.com.

S.I.1. Characterization Techniques and Materials

The product's crystallinity was evaluated using X-ray diffraction (XRD) with a Bruker XRD D2 Phaser (Billerica, MA, USA, λ = 1.540 Å). Raman spectra were recorded at room temperature with the aid of a DXR Raman spectrometer from Thermo Scientific (Waltham, MA, USA). The functional groups present in the synthesized material were analyzed using Fourier Transform Infrared (FT-IR) spectroscopy. To explore the structural conformation of the synthesized nanocomposite, various techniques were employed, including Field Emission Scanning Electron Microscopy (FESEM, JEOL-JSM7610F) and Transmission Electron Microscopy (TEM, H-7600, Hitachi, Japan). Additionally, Energy-Dispersive X-ray Spectroscopy (EDX) was employed to investigate the chemical composition and quantity of the elements present. The BET− Micrometric ASAP 2020M was utilized to evaluate the active surface area and the average diameter of the pore. X-ray photoelectron spectroscopy (XPS) was carried out with monochromatic Al Kα X-ray radiation as the excitation source on a Thermo ESCLAB 250 instrument to evaluate the oxidation state and identify metal sites. To investigate the surface charge of the material through zeta potential, Beckman Coulter Delsa Nano C. Additionally, electrochemical analysis, which included electrochemical impedance spectroscopy (EIS), was performed using a CHI 1211B workstation (CH Instruments, Inc., Austin, TX, USA). All experiments were executed within a standard three-electrode system. praseodymium (III) nitrate hexahydrate ($Pr(NO_3)_3 \cdot 6H_2O$), sodium tungstate dihydrate ($Na_2WO_4 \cdot 2H_2O$), Furaltadone, sodium phosphate dibasic anhydrous (NaH_2PO_4), and sodium phosphate monobasic dihydrate ($NaH_2PO_4 \cdot 2H_2O$) from Sigma-Aldrich.

Additionally, Dysprosium (III) nitrate hexahydrate ($Dy(NO_3)_3 \cdot 5H_2O$), tin (II) chloride ($SnCl_4$), ammonium hydroxide (NH_4OH), and urea ($CO(NH_2)_2$) from Sigma-Aldrich and CTAB ($C_{19}H_{42}BrN$) from Alfa Aesar were purchased and used directly without any purification process.

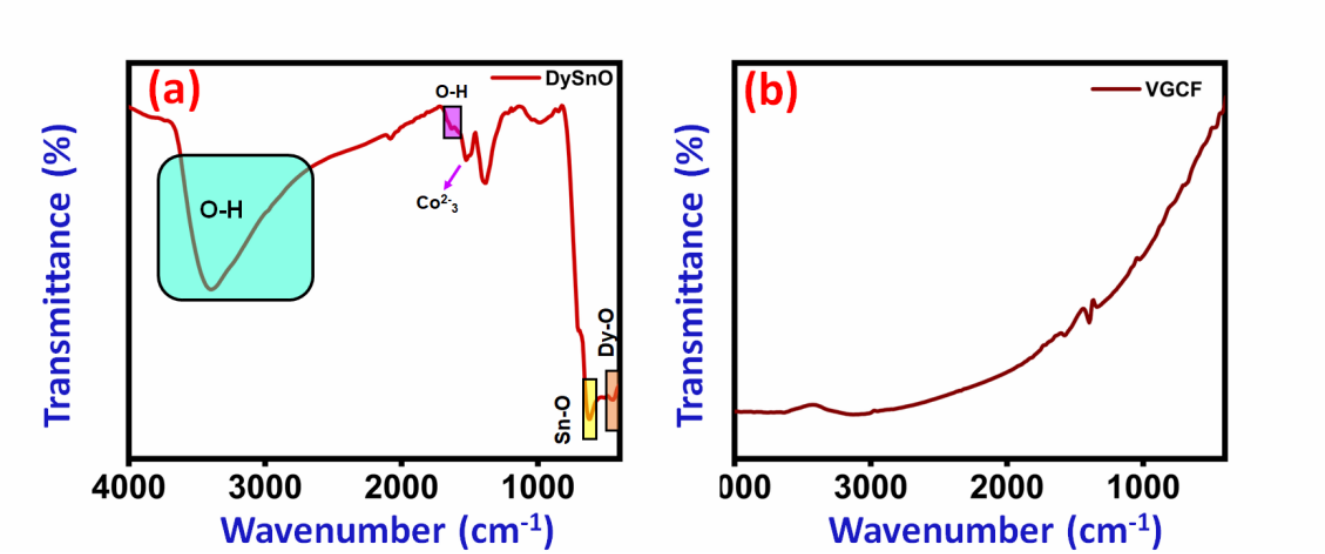

Figure S1: FTIR spectra of DySnO (a) and VGCF (b)

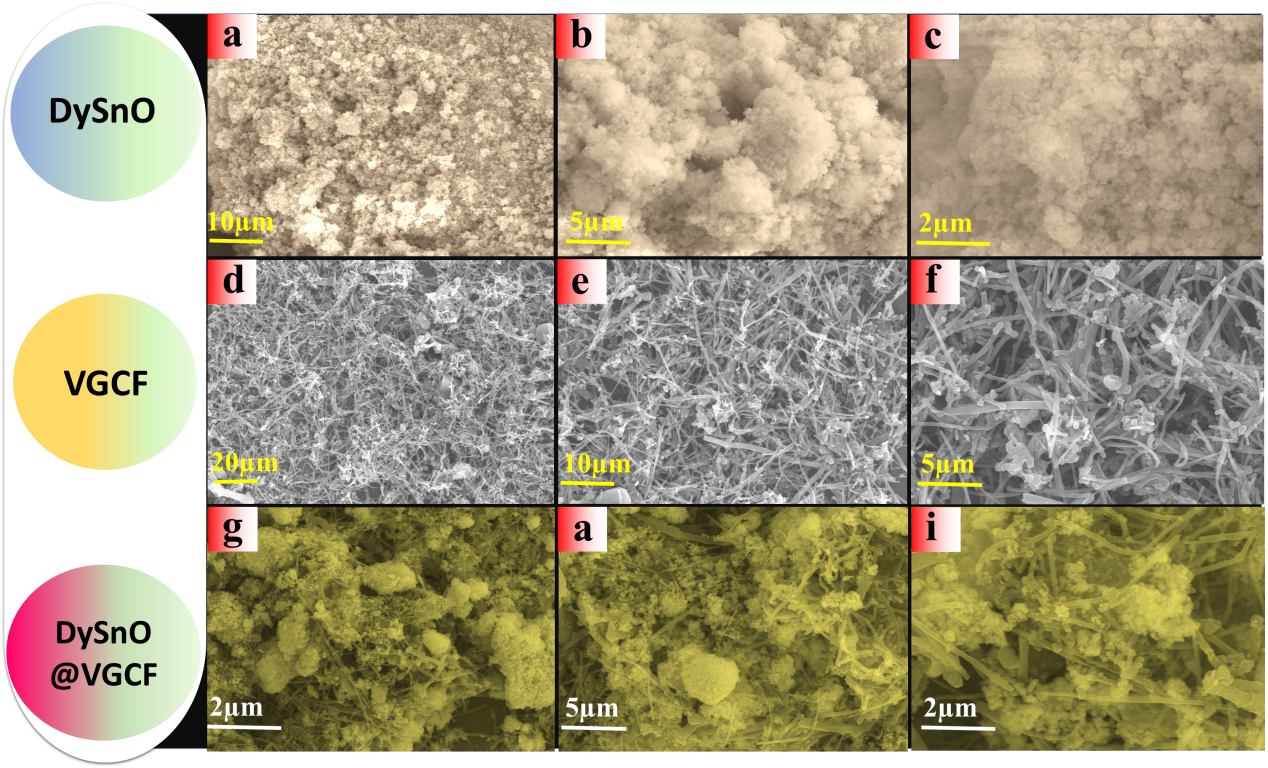

Figure S2: FESEM images of DySnO, VGCF and DySnO@VGCF nanocomposite at different magnifications (a) 10µm, (b) 5µm, (c) 2µm (d); (a) 20µm, (b) 10µm, (c) 5µm; (a) 2µm (b) 5µm (c) 2µm respectively.

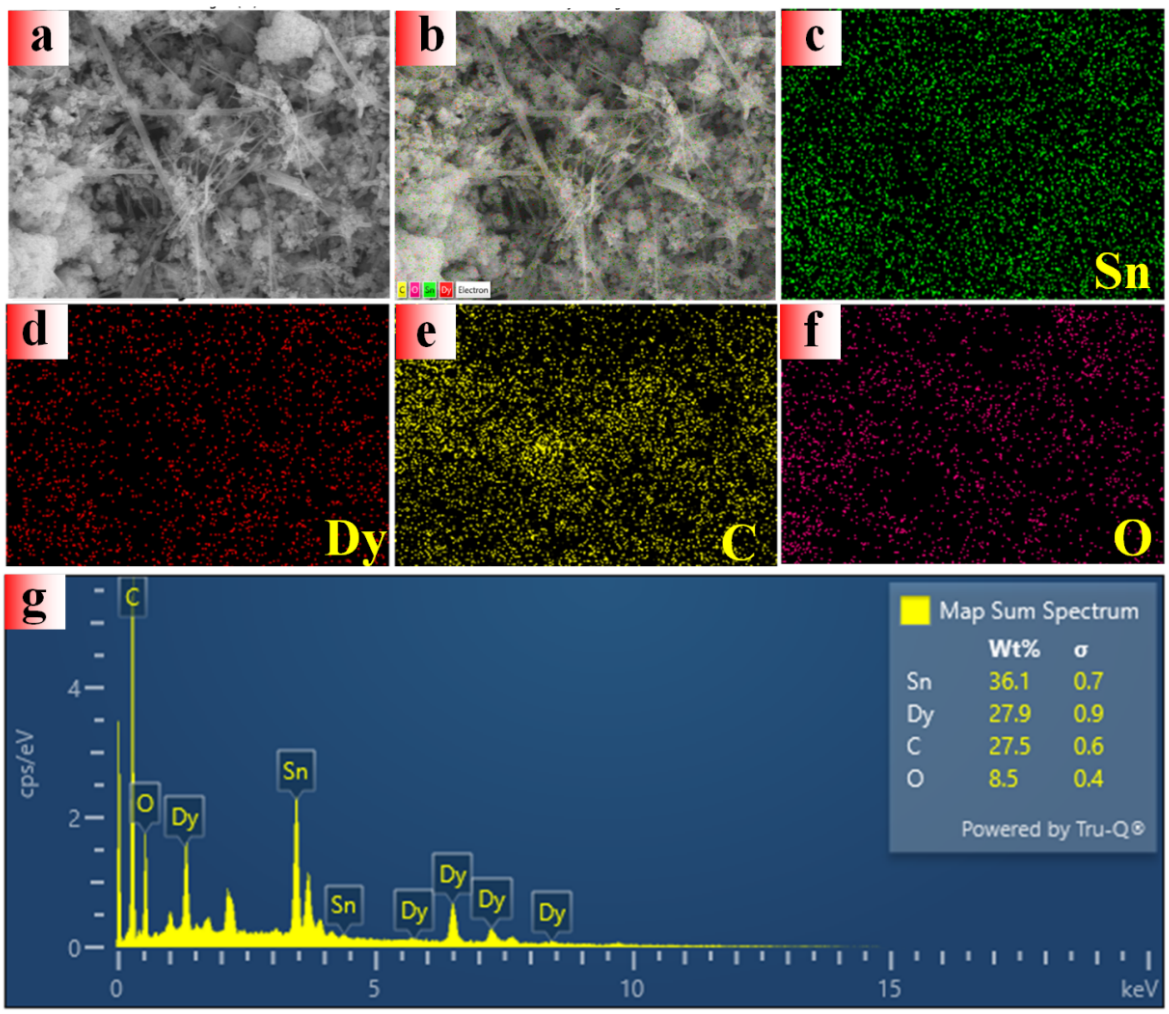

Figure S3: Elemental mapping images of Sn, Dy, C and O and EDX spectra of $Dy_2Sn_2O_7$@VGCF Composite materials, respectively.

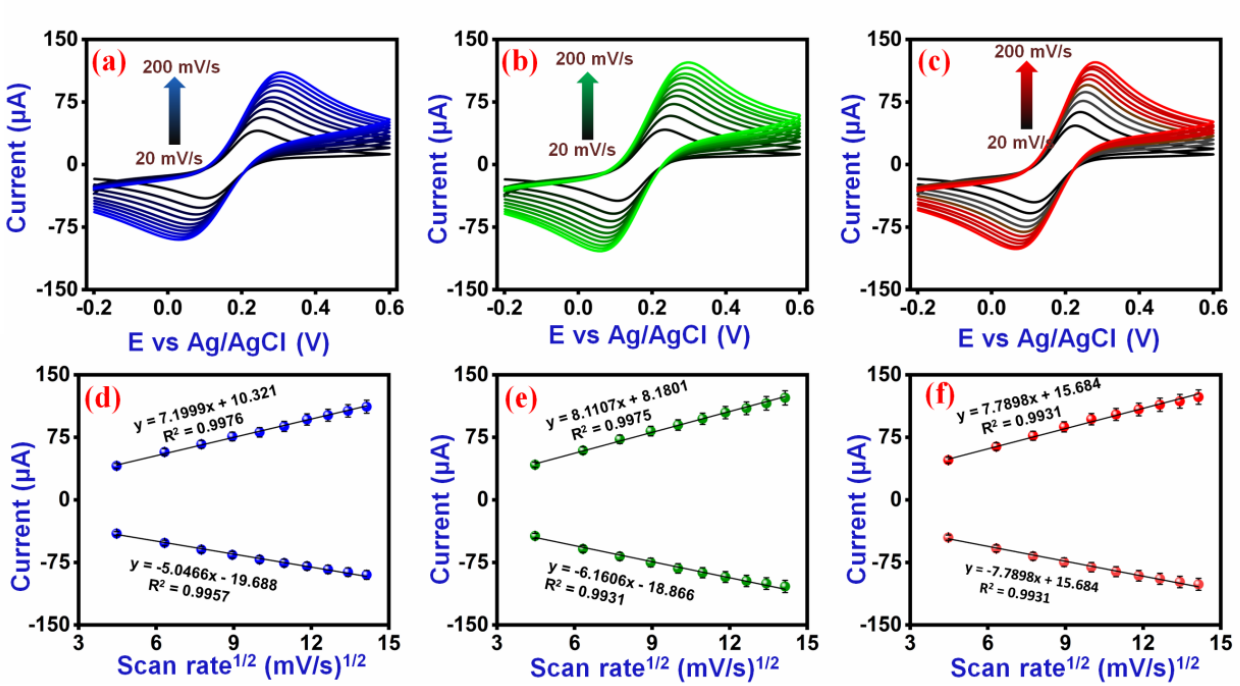

Figure S4: CV curves of (a) bare GCE (b) DySnO/GCE and (c) VGCF/GCE in a solution containing 0.1 M KCl in 5 mM $[Fe(CN)_6]^{3-/4-}$ at different scan rates (d-f) corresponding linear plot of bare (a) bare GCE, (b) DySnO/GCE, and (c) VGCF/GCE, respectively.

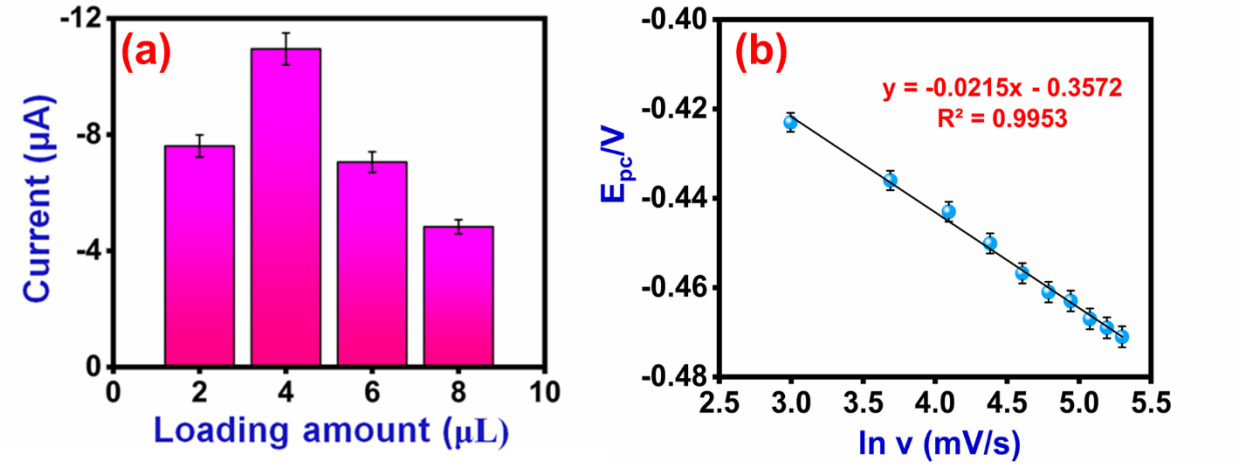

Figure S5: (a) Bar representation of different loading. (b) Linear plot of ln (scan rate (mV/s)) vs. cathodic peak potential.

Additionally, the Laviron theory establishes the relation between the peak potential and the logarithm of scan rate, as shown in **Fig S5.** Conversely, the equations (1&2) allow to identify the number of electrons transferred during the reduction of FLD at the surface of DySnO@VGCF/GCE.

$$\mathbf{E_{pc}\ [v] = -0.3572\ \left[\frac{mV}{s}\right] - 0.0215,\ (R^2=0.9953)} \text{ ----------(1)}$$

$$E_p = E^{o'} + \left(\frac{RT}{\alpha nF}\right) ln\left(\frac{RTK^o}{\alpha nF}\right) + \left(\frac{RT}{\alpha nF}\right) ln[v\left(\frac{mV}{s}\right)] \text{ ----------(2)}$$

where K^0 is the standard rate constant, n is the number of electrons captured by the FLD molecules at the moment of the reduction reaction on the electro-catalytic surface of our constructed sensor, R is the constant of perfect gas (8.31 SI), T is the room temperature (298 K), $E^{0'}$ is the formal potential, F is the stack constant (96,500C), and α is the electron transfer coefficient (0.5). Finally, the number of electrons that are transferred at the surface of DySnO@VGCF/GCE sensor is found to be 4.

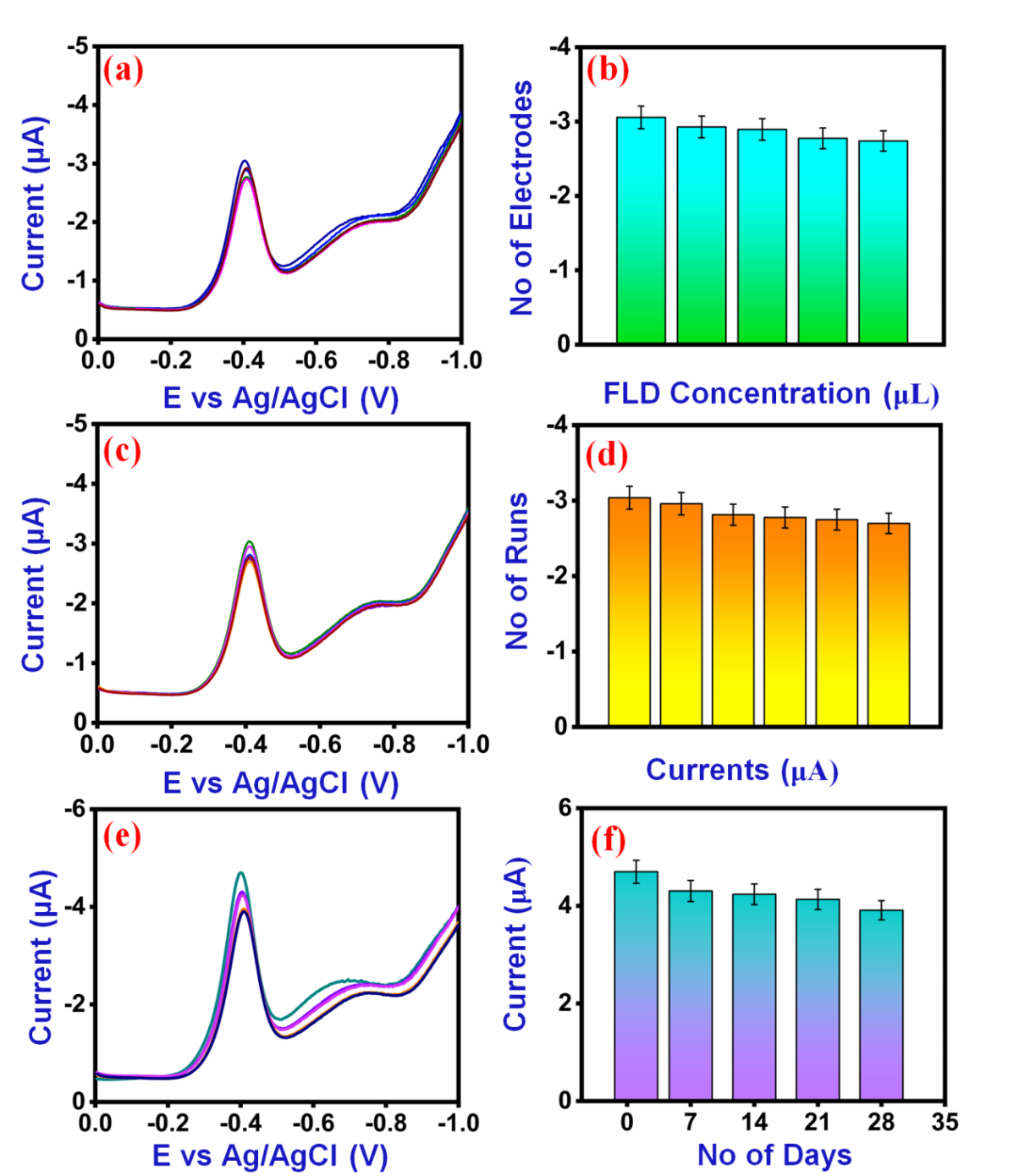

Figure S6: (a) DPV measurements for reproducibility investigations at $Dy_2Sn_2O_7$@VGCF modified glassy carbon electrode (GCE), (b) bar graph comparing various modified electrodes against peak current, (c) DPV measurements for the repeatability test at $Dy_2Sn_2O_7$@VGCF modified GCE, (d) bar graph illustrating peak current in relation to the number of repetitions), (e) Assessment of storage stability for the modified electrode at $Dy_2Sn_2O_7$@VGCF on GCE (f) line graph representing days of storage versus peak current.

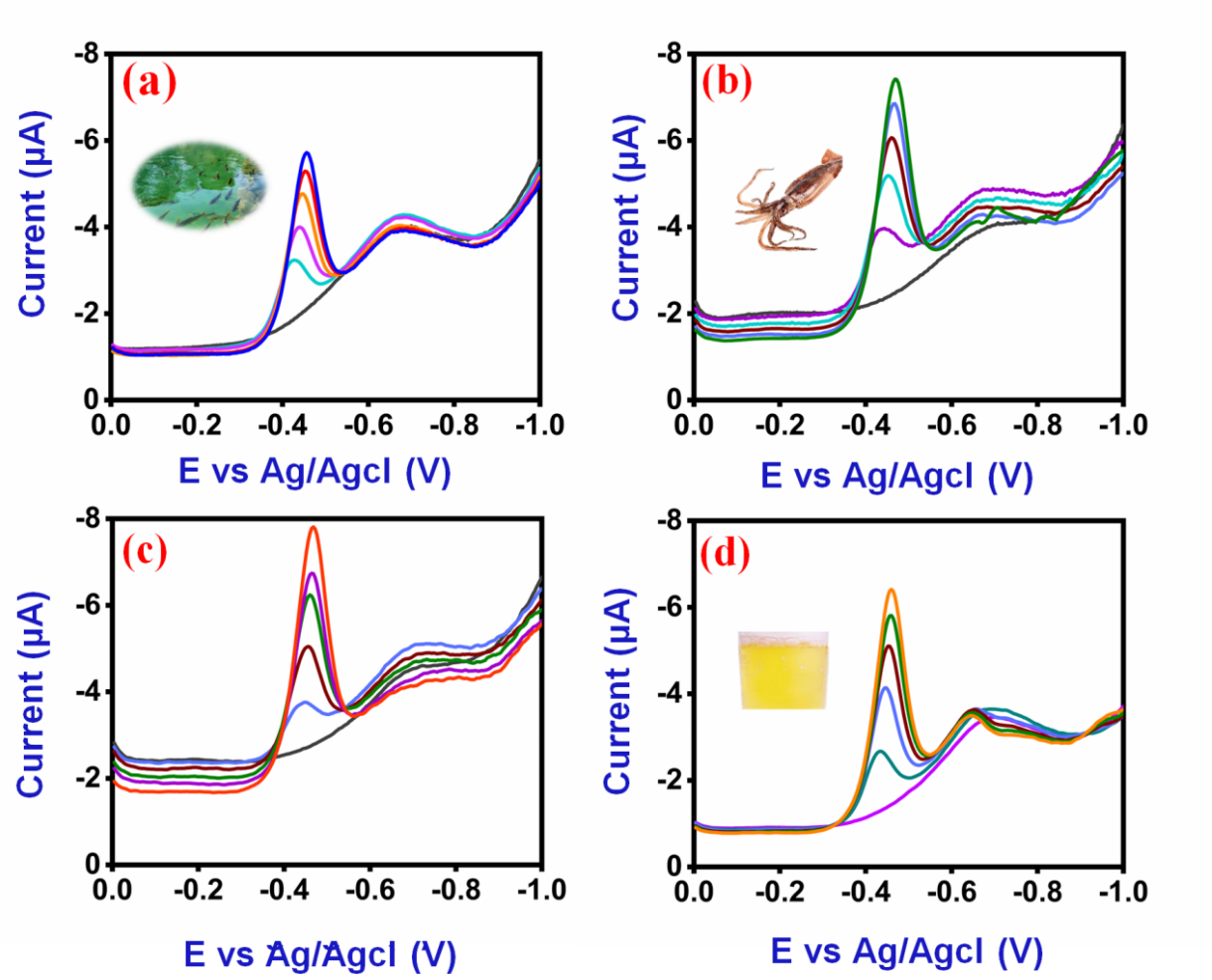

Figure S7: Real Sample Analysis of fish culture water (a), squid (b), pond water (c), and urine samples (d).

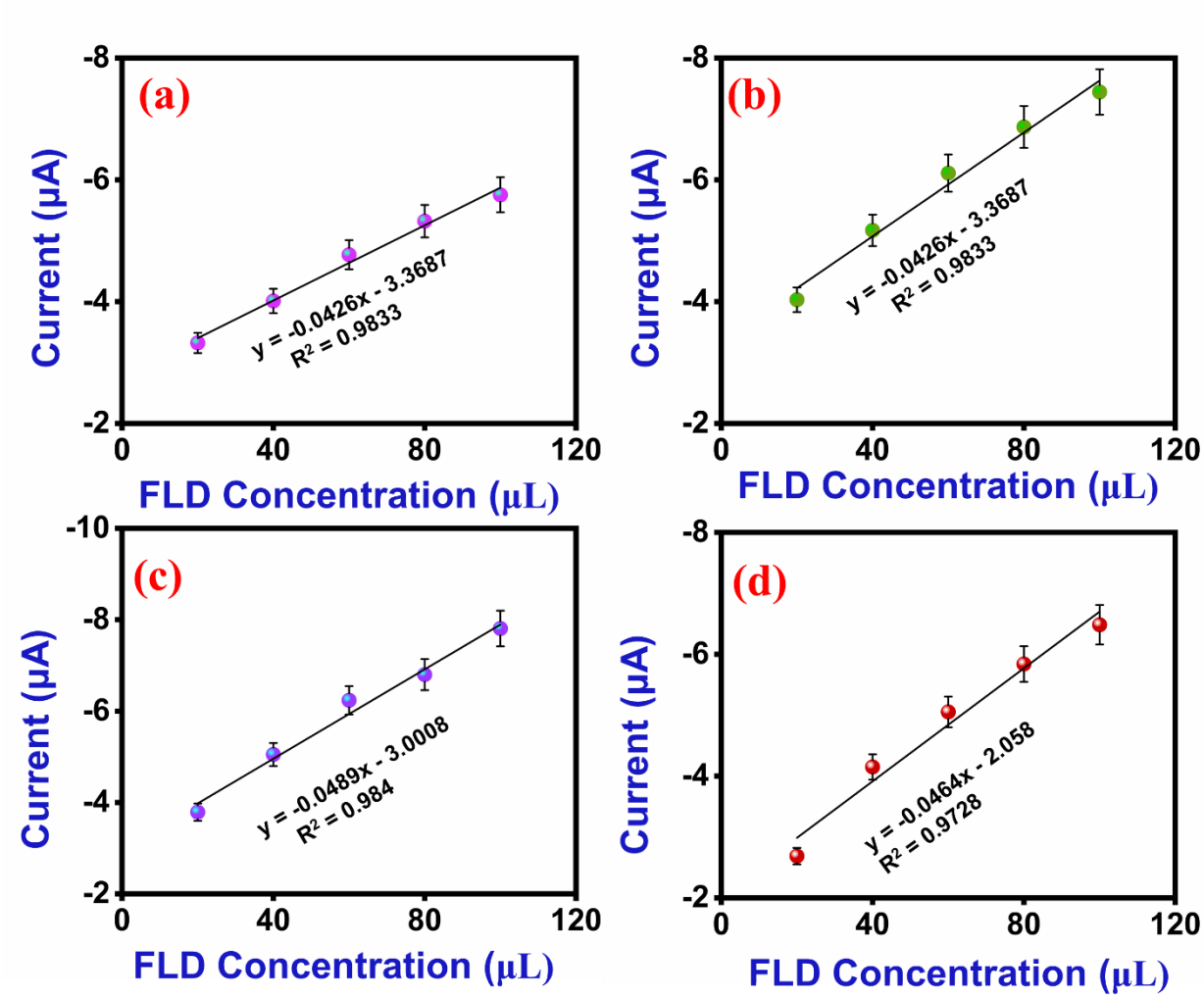

Figure S8: Corresponding calibration plots for the real samples.

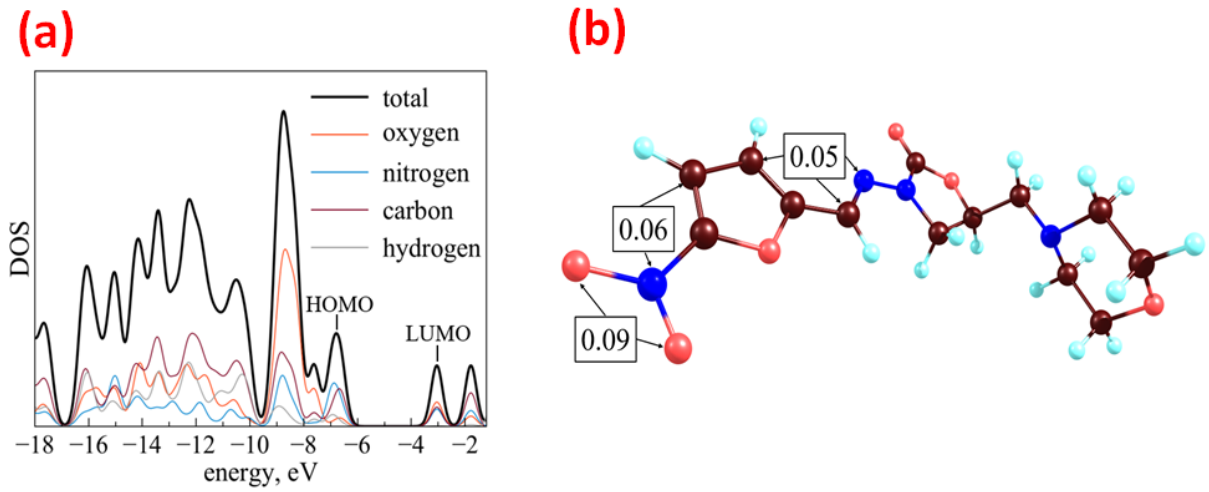

Figure S9: (a) DOS / projected DOS (*b*) of FLD. Gauss broadening with FWHM = 0.5 eV is applied to all molecular energy levels (b) Fukui indexes of the most active FLD atoms with f_i > 0.05.

Table S1. Recovery ranges of real sample analysis

Sample	Added (uL)	Found	Recovery (%)	RSD% (n=3)
Fish Culture Water	20	-3.323	97.05	-0.101
	40	-4.011	97.33	-0.11
	60	-4.77	95.78	-0.21
	80	-5.322	98.13	-0.101
	100	-5.754	98.05	-0.114
Squid	20	-4.031	99.16	-0.032
	40	-5.171	98.05	-0.1
	60	-6.11	98.73	-0.08
	80	-6.868	99.21	-0.054
	100	-7.442	98.86	-0.09
Pond Water	20	-3.789	99.16	-0.032
	40	-5.05	98.05	-0.1
	60	-6.236	98.73	-0.08
	80	-6.798	99.21	-0.054
	100	-7.807	98.86	-0.09
Urine Sample	20	-2.687	96.44	-0.099
	40	-4.15	98.10	-0.08
	60	-5.053	97.88	-0.109
	80	-5.84	98.63	-0.081
	100	-6.483	99.14	-0.056